AIP Advances

A novel metamaterial filter with stable passband performance based on frequency selective surface

C. Y. Fang, J. S. Gao, and Hai Liu

Citation: AIP Advances **4**, 077114 (2014); doi: 10.1063/1.4890108
View online: http://dx.doi.org/10.1063/1.4890108
View Table of Contents: http://scitation.aip.org/content/aip/journal/adva/4/7?ver=pdfcov
Published by the AIP Publishing

AIP ADVANCES **4**, 077114 (2014)

A novel metamaterial filter with stable passband performance based on frequency selective surface

C. Y. Fang,[a] J. S. Gao, and Hai Liu
Optical system Key Laboratory of Advanced Manufacturing Technology, Changchun Institute of Optics, Fine Mechanics and Physics Institute, Changchun, 130033, China

(Received 18 March 2014; accepted 2 July 2014; published online 11 July 2014)

In this paper, a novel metamaterial filter based on frequency selective surface (FSS) is proposed. Using the mode matching method, we theoretically studied the transmission performance of the structure. Results show that, by rotating its neighboring elements 90 degree, the novel filter has a better stability to angle of incidence than traditional structures for TE and TM polarization. As the incident angles vary from 0 to 50 degrees, the metamaterial filter exhibits a transmittance higher than 0.98 and the center frequency slightly shifts downward (from 10 GHz to 0.96 GHz) for TE polarization. For TM polarization, a transmittance of 0.98 is achieved and the center frequency retains 0.96 GHz with the varying of the incident angles. Furthermore, an experimental prototype fabricated was tested in a microwave chamber, and the measured results show good agreement with the simulated ones. [http://dx.doi.org/10.1063/1.4890108]

I. INTRODUCTION

Metamaterials are artificially constructed electromagnetic (EM) materials with engineered electric permittivity and magnetic permeability[1] obtained through geometrically structuring natural materials, such as metals, semiconductors and insulators. They have exotic EM responses not available in nature and consequently have been applied in many aspects, such as negative refractive index,[2,3] superlens,[4] cloaking[5,6] and thermal emitters.[7] Metamaterials containing Frequency Selective Surfaces (FSSs) can have an excellent resonance frequency performance, not only in existence but also in design. A FSS is a two dimensional structure composed of a periodic array of metal-patched or periodic opening units on a metallic screen, which acts as a spatial filter with band stop or band pass capability.[8,9] Many techniques have been presented to improve the resonance frequency stability performance, including choosing proper FSS elements and arrays, increasing the thickness of the supporting dielectric layer and metallic screen, and so on. Widenberg *et al*. analyzed and simulated the transmission performances of the circle and hexagon thick-screen FSS structures using the mode matching method.[10] He believe that irises at the apertures stabilize passband for different incident angles; the bandwidth decreases when the thickness of the aperture layer is increased and when the permittivity of the aperture layer is increased. Fang *et al*. analyzed and simulated the transmission performance of a circular aperture thick-screen FSS structure with dielectric using mode matching method and moment method.[11] Tang *et al*. analyzed and simulated a novel four-legged loaded element thick-screen FSS with stable performances.[12] However, they cannot give a structure with stable passband performance for different polarization wave. Hence, in this paper we design a novel metamaterial based on the FSS in order to obtain stable passband performances for different polarization wave at large incident angles.

[a]f_y_u@sina.com

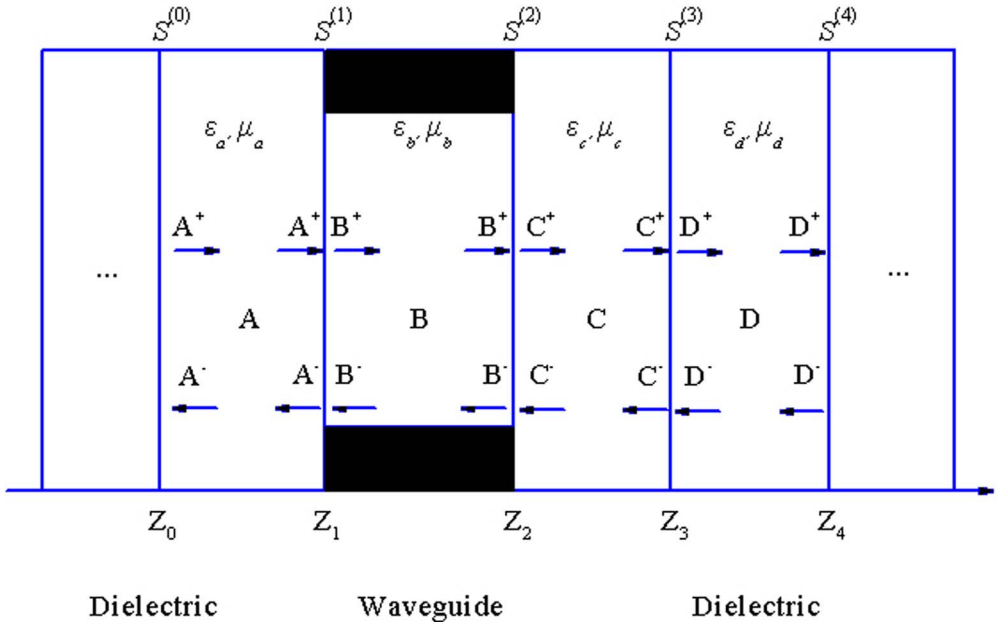

FIG. 1. Equivalent mathematical models for analyzing a FSS.

II. PRINCIPLES AND ANALYSIS

One of the important factors influencing the metamaterial response frequency is the design of the FSS, including its element shape, size and array spacing. As a plane wave impinges on the FSS, its transmission performance can be analyzed using the mode matching method.

Firstly, we establish an equivalent mathematical model. The model consists of dielectric regions **A**, **C**, **D**, waveguide region **B**, and the interfaces between the dielectric regions and the waveguide region, as well as the interfaces between the dielectric regions, as shown in Figure 1.

When the electromagnetic wave passes through dielectric layer **A**, the scattering coefficients on each side

$$\begin{cases} \mathbf{A}^{+}_{mn}(z_1) = I \cdot e^{i\cdot\gamma_{mn}(z_1-z_0)} \cdot \mathbf{A}^{+}_{mn}(z_0), \\ \mathbf{A}^{-}_{mn}(z_1) = I \cdot e^{i\cdot\gamma_{mn}(z_1-z_0)} \cdot \mathbf{A}^{-}_{mn}(z_0). \end{cases} \tag{1}$$

When the electromagnetic wave passes through waveguide **B**, the scattering coefficients on each sides

$$\begin{cases} \mathbf{B}^{+}_{mn}(z_2) = I \cdot e^{i\cdot\gamma_{mn}(z_2-z_1)} \cdot \mathbf{B}^{+}_{mn}(z_1), \\ \mathbf{B}^{-}_{mn}(z_2) = I \cdot e^{i\cdot\gamma_{mn}(z_2-z_1)} \cdot \mathbf{B}^{-}_{mn}(z_1). \end{cases} \tag{2}$$

In the case of an interface between two different dielectrics, the fields inside **C** and **D** can be expanded in Floquet mode as

$$\begin{cases} \mathbf{E}^{c}_{T}(\mathbf{r}) = \sum_{lmn} (c^{+}_{lmn} e^{i\gamma^{c}_{mn} z} + c^{-}_{lmn} e^{-i\gamma^{c}_{mn} z}) \mathbf{R}^{c}_{Tlmn}(\boldsymbol{\rho}), \\ \mathbf{H}^{c}_{T}(\mathbf{r}) = \sum_{lmn} (c^{+}_{lmn} e^{i\gamma^{c}_{mn} z} - c^{-}_{lmn} e^{-i\gamma^{c}_{mn} z}) \mathbf{T}^{c}_{Tlmn}(\boldsymbol{\rho}), \end{cases} \quad (z < z_3), \tag{3}$$

$$\begin{cases} \mathbf{E}^{d}_{T}(\mathbf{r}) = \sum_{lmn} (d^{+}_{lmn} e^{i\gamma^{d}_{mn} z} + d^{-}_{lmn} e^{-i\gamma^{d}_{mn} z}) \mathbf{R}^{d}_{Tlmn}(\boldsymbol{\rho}), \\ \mathbf{H}^{d}_{T}(\mathbf{r}) = \sum_{lmn} (d^{+}_{lmn} e^{i\gamma^{d}_{mn} z} - d^{-}_{lmn} e^{-i\gamma^{d}_{mn} z}) \mathbf{T}^{d}_{Tlmn}(\boldsymbol{\rho}), \end{cases} \quad (z > z_3), \tag{4}$$

where **E** and **H** are the waveguide mode, and **R** and **T** represent the Floquet mode of the electric field and the magnetic field respectively. The boundary conditions at the interface between **C** and **D** ensure that the tangential electric and magnetic field are continuous over the entire interfaces K, are enforced.

$$\begin{cases} \mathbf{E}_T^c(\boldsymbol{\rho}, z_3) = \mathbf{E}_T^d(\boldsymbol{\rho}, z_3), \\ \mathbf{H}_T^c(\boldsymbol{\rho}, z_3) = \mathbf{H}_T^d(\boldsymbol{\rho}, z_3), \end{cases} \boldsymbol{\rho} \in K. \tag{5}$$

The elements of the scattering matrix are

$$\begin{cases} S_{11}^3 = -(\mathbf{R}^c + \mathbf{G}^t\mathbf{R}^{d*-1}\mathbf{G}^*)^{-1}(\mathbf{R}^c - \mathbf{G}^t\mathbf{R}^{d*-1}\mathbf{G}^*), \\ S_{12}^3 = 2(\mathbf{R}^c + \mathbf{G}^t\mathbf{R}^{d*-1}\mathbf{G}^*)^{-1}\mathbf{G}^t, \\ S_{21}^3 = 2(\mathbf{R}^{d*} + \mathbf{G}^*\mathbf{R}^{c-1}\mathbf{G}^t)^{-1}\mathbf{G}^*, \\ S_{22}^3 = (\mathbf{R}^{d*} + \mathbf{G}^*\mathbf{R}^{c-1}\mathbf{G}^t)^{-1}(\mathbf{R}^{d*} - \mathbf{G}^*\mathbf{R}^{c-1}\mathbf{G}^t), \end{cases} \tag{6}$$

where * denotes complex conjugate. The fields inside the dielectrics are expanded in Floquet mode as

$$\begin{cases} \mathbf{E}_T^a(\mathbf{r}) = \sum_{lmn} (a_{lmn}^+ e^{i\gamma_{mn}^a z} + a_{lmn}^- e^{-i\gamma_{mn}^a z})\mathbf{R}_{Tlmn}^a(\boldsymbol{\rho}), \\ \mathbf{H}_T^a(\mathbf{r}) = \sum_{lmn} (a_{lmn}^+ e^{i\gamma_{mn}^a z} - a_{lmn}^- e^{-i\gamma_{mn}^a z})\mathbf{T}_{Tlmn}^a(\boldsymbol{\rho}), \end{cases} (z_0 < z < z_1), \tag{7}$$

and the fields inside waveguide are expanded in waveguide modes as

$$\begin{cases} \mathbf{E}_T^b(\mathbf{r}) = \sum_{vn} (b_{vn}^+ e^{ik_{zn}^b z} + b_{vn}^- e^{-ik_{zn}^b z})\mathbf{E}_{Tvn}^b(\boldsymbol{\rho}), \\ \mathbf{H}_T^b(\mathbf{r}) = \sum_{vn} (b_{vn}^+ e^{ik_{zn}^b z} - b_{vn}^- e^{-ik_{zn}^b z})\mathbf{H}_{Tvn}^b(\boldsymbol{\rho}), \end{cases} (z_1 < z < z_2). \tag{8}$$

Enforcing the continuity condition of the field at the interface $Z = Z_1$ yield

$$\begin{cases} \sum_{lmn} \left[A_{lmn}^+(z_1) + A_{lmn}^-(z_1)\right] \cdot \mathbf{R}_{Tlmn}^a(\boldsymbol{\rho}) = \begin{cases} \sum_{vn} \left[B_{vn}^+(z_1) + B_{vn}^-(z_1)\right] \cdot \mathbf{E}_{Tvn}^b(\boldsymbol{\rho}), (\boldsymbol{\rho} \in \Omega), \\ 0, \qquad\qquad (\boldsymbol{\rho} \in L \backslash \Omega), \end{cases} \\ \sum_{lmn} \left[A_{lmn}^+(z_1) - A_{lmn}^-(z_1)\right] \cdot \mathbf{T}_{Tlmn}^a(\boldsymbol{\rho}) = \sum_{vn} \left[B_{vn}^+(z_1) - B_{vn}^-(z_1)\right] \cdot \mathbf{H}_{Tvn}^b(\boldsymbol{\rho}), \ (\boldsymbol{\rho} \in \Omega). \end{cases} \tag{9}$$

The elements of the scattering matrix are

$$\begin{cases} S_{11}^1 = -(\mathbf{R} + \mathbf{G}^t\mathbf{Q}^{*-1}\mathbf{G}^*)^{-1}(\mathbf{R} - \mathbf{G}^t\mathbf{Q}^{*-1}\mathbf{G}^*), \\ S_{12}^1 = 2(\mathbf{R} + \mathbf{G}^t\mathbf{Q}^{*-1}\mathbf{G}^*)^{-1}\mathbf{G}^t, \\ S_{21}^1 = 2(\mathbf{Q}^* + \mathbf{G}^*\mathbf{R}^{-1}\mathbf{G}^t)^{-1}\mathbf{G}^*, \\ S_{22}^1 = (\mathbf{Q}^* + \mathbf{G}^*\mathbf{R}^{-1}\mathbf{G}^t)^{-1}(\mathbf{Q}^* - \mathbf{G}^*\mathbf{R}^{-1}\mathbf{G}^t). \end{cases} \tag{10}$$

Similarly, the linear system for the scattering coefficients at the interface between the waveguide **B** and dielectric **C** are

$$\begin{bmatrix} \mathbf{B}^-(z_2) \\ \mathbf{C}^+(z_2) \end{bmatrix} = \underbrace{\begin{bmatrix} S_{11}^2 & S_{12}^2 \\ S_{21}^2 & S_{22}^2 \end{bmatrix}}_{S^2} \begin{bmatrix} \mathbf{B}^+(z_2) \\ \mathbf{C}^-(z_2) \end{bmatrix}, \tag{11}$$

where the elements of the scattering matrix S are

$$S_{11}^1 = S_{22}^2, \quad S_{12}^1 = S_{21}^2, \quad S_{21}^1 = S_{12}^2, \quad S_{22}^1 = S_{11}^2. \tag{12}$$

Finally, one can obtain the transmission coefficient matrix of the FSS.

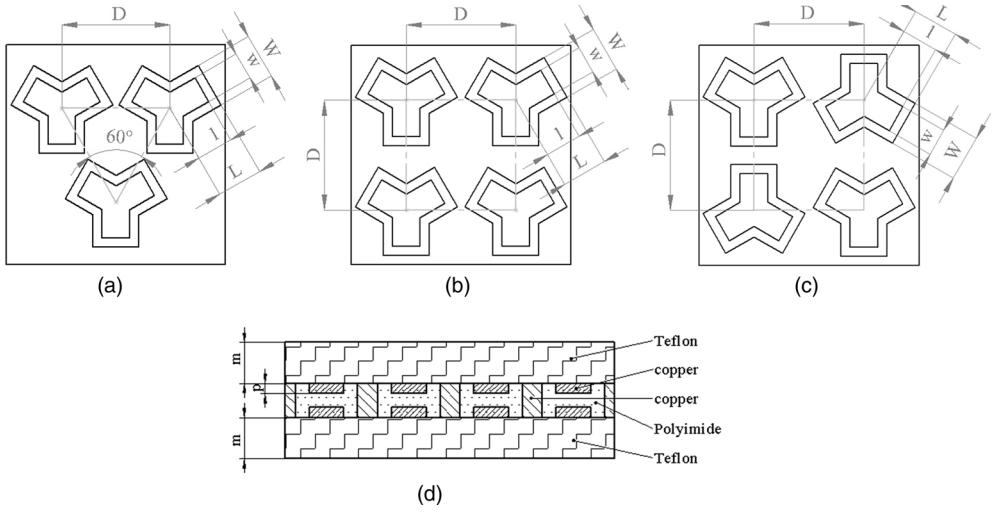

FIG. 2. Grid and element geometry of a FSS: (a) traditional triangle array, (b) traditional square array, (c) turning arrays, (d) a cross-section.

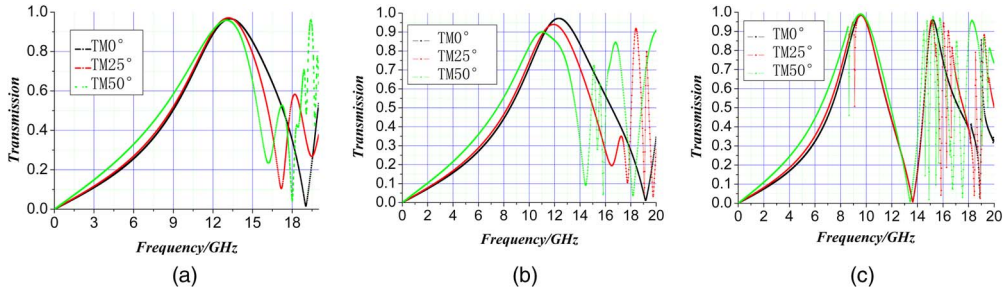

FIG. 3. Calculated TM transmission curves for (a) triangle array, (b) square array, (c) turning array.

In the above discussion, $\mathbf{A}^{\pm}$, $\mathbf{B}^{\pm}$, $\mathbf{C}^{\pm}$, $\mathbf{D}^{\pm}$ are the unknown coefficient matrixes. $\mathbf{R}_{Tlmn}$ and $\mathbf{T}_{Tlmn}$ are the coefficients of reflection and transmission, respectively; $R^{*}_{Tl'm'n'}$ and $\mathbf{T}^{*}_{Tl'm'n'}$ are conjugate complex numbers; The letter a, b, c, and d are superscripts of various layers. $\mathbf{E}_{Tvn}$ and H_{Tvn} are the electric fields and magnetic fields, respectively; $\mathbf{E}^{*}_{Tvn}$ and H^{*}_{Tvn} are their conjugate complex numbers; k is the propagation constant of an incident plane wave, γ is the propagation constant of Floquet wave.

III. SIMULATIONS AND DISCUSSIONS

Compared to the traditional FSS of triangle or square element array, the neighboring Y-hole elements of the novel metamaterial are rotated by 90 degree, as shown in Figure 2. The dimensions are L = 5 mm, l = 4 mm, W = 5 mm, w = 3 mm, D = 12 mm, m = 1.5 mm, n = 0.5 mm, p = 0.03 mm. By turning the Y-hole elements, the element array pattern of the novel metamaterial are changed correspondingly, and a stable frequency responses are observed at incidence angles from 0° to 50° for TE/TM polarization, which will be describe and analyzed in detail below.

A. Angular stability for TM polarization

Every element on the FSS can be regarded as an identical Y-hole waveguide element. The copper patches that form irises are placed at the apertures on either side of the copper plate. By using CST 2012, we simulate the resonant frequency of the above mentioned three type FSSs. Figure 3 shows their resonant frequencies for TM polarization at incidence angles of $\theta = 0°, 25°, 50°$. For the case

TABLE I. TM transmission properties for different element array.

Arrays	θ/°	f_0/GH	T	W/GH
	0	13.2	0.9653	5.44
triangle	25	13.1	0.9704	4.9
	50	13.0	0.9581	4.7
	0	12.1	0.9684	4.98
Square	25	11.8	0.9392	4.24
	50	11.0	0.8999	3.9
	0	9.60	0.9843	2.72
Turning	25	9.56	0.9845	2.9
	50	9.56	0.9893	1.76

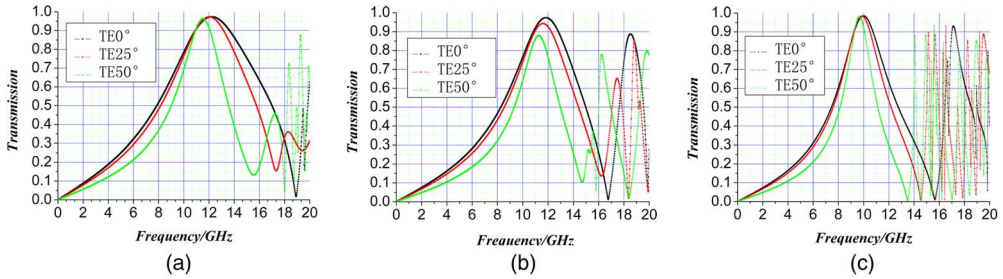

FIG. 4. Calculated TE transmission curves for (a) triangle array, (b) square array, (c) turning array.

of triangle array, with the increase of θ the centre frequency f_0 has a 0.2 GHz downward drift, the bandwidth W at −3dB decreases 0.74 GHz, and the transmittance T of centre frequency decreases 0.0072. For the square array, f_0 drifts 1.1 GHz downward, W reduces 1.08 GHz, and T decreases 0.0685. But for turning arrays, f_0 only has a drift of 0.04 GHz downward, W decreases 0.96 GHz, and T increases 0.005, as shown in Table I.

From Table I, it can be seen that the two traditional arrays have similar resonant frequency movement as the incidence angles increase. The centre frequency shifts downwards obviously; the bandwidth and transmittance decrease swiftly. But on the other hand, the turning array has a higher transmittance and a stable centre frequency. This is because in symmetrical structures the Y-hole elements acted as waveguide cavities and the field in the cavity can be equably distributed, then a stable resonance frequency is produced for the dominant mode and the TM high order mode. In the following, a vertical slot on the input plane of the FSS is used to select the horizontal polarization from the incident radiation. The energy coupled from the slot can excite the field in the cavity, and then outgoing wave is subsequently coupled out through an orthogonal slot. In this way, it is possible to introduce a desired 90 degree rotation of the polarization of the incident wave. Note that when the field distributions for the two modes are orthogonal to each other, the field effect on TM dominant mode is not the same as the field effect on TM high order mode. Therefore, the turning Y-holes result in a different field perturbation for the two modes.

B. Angular stability for TE polarization

Figure 4 illustrate the TE transmission lines for these three type FSSs at incidence angle $\theta = 0^\circ, 25^\circ, 50^\circ$. When the incident angle increases from 0° to 50°, for the case of triangle array, f_0 drifts 0.88 GHz downward, W reduces 3.2 GHz, and T decreases 0.0093. For the case of square array, f_0 drifts 0.5 GHz downward, W at -3dB reduces 1.42 GHz, and T decreases 0.0949. While for the case of turning array, f_0 drifts 0.34 GHz downward, W reduces 1.42 GHz, and T decreases 0.0048, as shown in Table II.

TABLE II. TE transmission properties for different element array.

Arrays	θ/°	f_0/GH	T	W/GH
	0	12.38	0.9725	5.94
Triangle	25	12.2	0.9709	4.88
	50	11.5	0.9632	2.74
	0	11.8	0.9737	3.18
Square	25	11.56	0.9429	2.76
	50	11.3	0.8788	1.76
	0	10	0.9848	3.18
Turning	25	9.86	0.9832	2.76
	50	9.66	0.9800	1.76

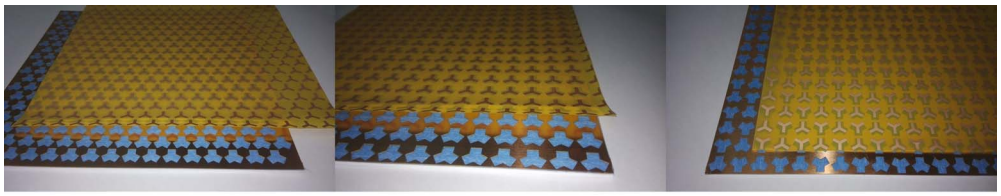

(a) (b) (c)

FIG. 5. A photograph of the FSS: (a) traditional triangle array, (b) traditional square array, (c) turning arrays, (d) a cross-section.

It can be seen that the metamaterial with the turning array has an additional advantage that the transmittance through the FSS is independent of the polarization of the source. The turning Y-holes can balance or change the field distribution given by a metallic screen, which is positioned at an appropriate distance away where the field is only negligibly influenced. Because the FSS element is symmetric under rotation of 90 degrees, both elements of polarization will "see" the same grid geometry. This means that the FSS with turning elements have the same transmission for TE/TM polarization wave, and the overall transmission coefficient is therefore not a function of the polarization angle and orientation.

IV. EXPERIMENTS AND COMPARISONS

To verify the above functionality, these three type FSSs are fabricated, as shown in Figure 5. The structures consist of 16×16 array of Y-hole elements on a copper plate (200 mm × 200 mm), which is sandwiched by two dielectric layer. The experimental setup used for measuring the proposed FSS is shown in Figure 6. A spot-focusing lens antenna and a vector network analyzer HP 8510C are used to measure the *S*-parameters. The measuring condition is as follow: the test background is less than -45dBsm and the scanning frequency range are 4 ∼ 12 GHz.

Figure 7 shows the comparison between the calculated and the measured transmission curves at incident angle 50° for TM/TE incident wave. We can see that the measured results for samples are consistent with the calculated value approximately. The small offset in resonance frequency curves is because the actual dimension of the FSS is finite. Inevitably, the finite size FSS leads to two problems: incidence wave illumination is not an absolutely flat plane; the antenna beam scattered at the edge of the FSS surface can produce edge diffraction effect.

In addition, simulations of the passband performance of the metamaterial filter have been performed using the frequency domain solver in CST Microwave Studio. The copper in material list as shown in Table III was substituted for PEC in order to decrease simulation time and maintain good accuracy of the results. A vertically polarized plane wave source was used to illuminate the surface at various angles of incidence. Magnetic periodic boundaries were placed along the surface length,

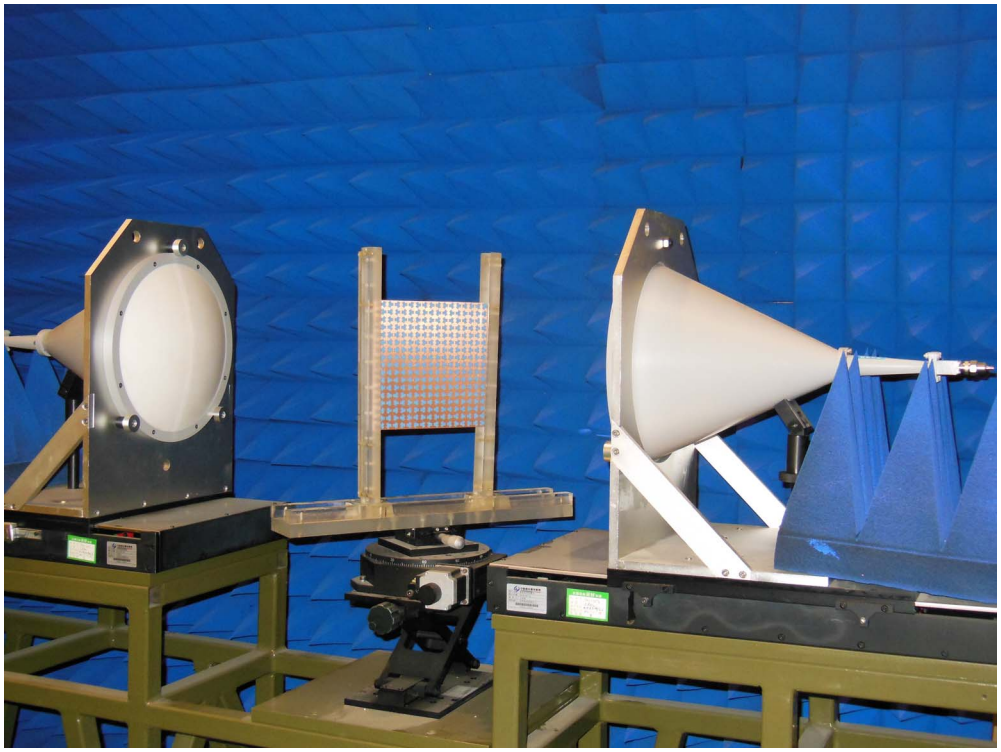

FIG. 6. A photograph of the microwave measurement system.

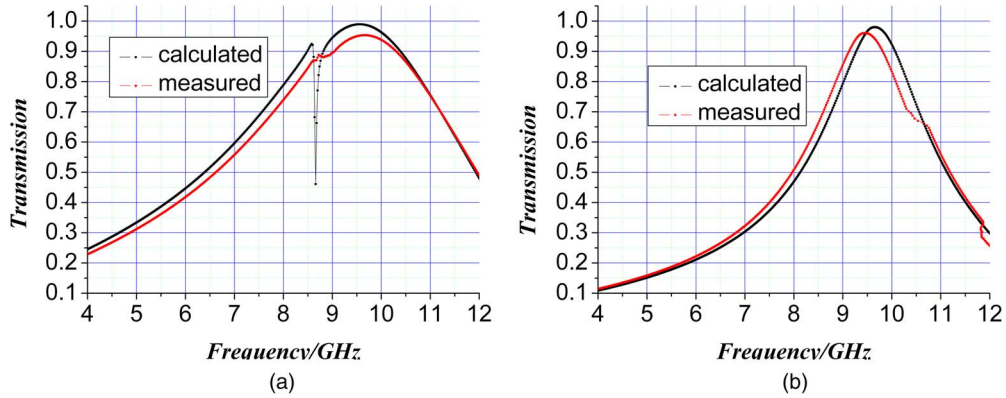

FIG. 7. Simulation and measurement curves at incidence angle 50° for: (a) the case of TM, (b) the case of TE.

TABLE III. Material specification for simulation and fabrication.

Material	Permittivity ε_r	Loss angle tangent tanθ
Teflon	2.15	0.008
Copper/PEC		
Polyimide	3.05	0.005

so the structure could be assumed to be infinitely wide when simulated. The computer hardware mainly includes that CPU frequency is 3.2 GHz and RAM capacity is 16 GB. The computational statistics related to simulation is as follow: total solver time is 613s; number of threads used is 4; number of mesh cells is 30455; accuracy is 5.15046e-005.

V. CONCLUSION

We design a metamaterial filter by rotating the neighboring elements on the FSS 90 degree. The novel structure has stable passband performances and high transmittances for different polarization orientations and incidence wave angles, which is attributed to the inter transmission field change of the structure induced by the rotation of neighboring elements. For 0, 25, 50 degree incidence angles, the metamaterial filter shows transmittances higher than 0.98 and the center frequency shifts less than 0.4 GHz for TE and TM wave. Furthermore, the bandwidth of the metamaterial filter's emission band can be stabilized by adequately tuning the geometrical and electrical parameters of the structure. The angular stability of the filter structure is finally addressed presenting simple design criteria to achieve good transmission performance at very wide incidence angles. Finally, by testing the experimental parts fabricated in a microwave chamber, we can see a good agreement between the simulations and experimental results.

ACKNOWLEDGMENTS

This work was supported by the innovation funded projects of the Changchun Institute of Optics, Fine Mechanics, and Physics, Chinese Academy of Sciences (ID:093Y32J090). The author would like to thank Dr. Gao Jinsong for valuable advices regarding the investigation. In addition, I also thank Dr. Sun Lianchun and Liu Hai for critical reviews of the manuscript.

[1] J. B. Pendry, IEEE Trans. Microw. Theory Tech. **47**, 2075 (1999).
[2] D. R. Smith, Science **305**, 788 (2004).
[3] J. Valentine, Nature **455**, 376 (2008).
[4] M. G. Silveirinha, Phys. Rev. B **81**, 033101 (2010).
[5] D. Schurig, Science **314**, 977 (2006).
[6] W. S. Cai, Nature Photon **1**, 224 (2007).
[7] X. L. Liu, Phys. Rev. Lett. **107**, 045901 (2011).
[8] B. A. Munk, *Frequency Selective Surfaces Theory and Design* (Wiley, New York, 2000), pp. 22–49.
[9] T. K. Wu, *Frequency Selective Surface and Grid Array* (Wiley, New York, 1995), pp. 149–203.
[10] B. Widenberg *et al.*, Journal of Electromagnetic Waves and Applications **14**, 1303 (2000).
[11] Chunyi Fang *et al.*, Acta. Phys. Sin. **59**, 5023 (2010).
[12] Guangming Tang *et al.*, Acta. Phys. Sin. **61**, 118401 (2012).